Coherent artifact and time-dependent polarization in amplified ultrafast erbium-doped fibre lasers

Miguel López-Ripa[1*], Benjamín Alonso[1], Sebastián Jarabo[2], Francisco J. Salgado-Remacha[2], Juan Carlos Aguado[3] and Íñigo J. Sola[1]

[1]Grupo de Aplicaciones del Láser y Fotónica (ALF), Departamento de Física Aplicada, University of Salamanca, Plaza de la Merced s/n 37008 Salamanca, Spain

[2]Departamento de Física Aplicada, Facultad de Ciencias, Universidad de Zaragoza, C/Pedro Cerbuna 12, 50009 Zaragoza, Spain

[3]Grupo de Comunicaciones Ópticas, Escuela Técnica Superior de Ingenieros de Telecomunicación, University of Valladolid, Paseo de Belén 15 47011 Valladolid, Spain

Author e-mail address: miguellr@usal.es*

Abstract

Mode-locked erbium-doped fibre lasers are ultrashort pulsed sources widely studied due to their versatility and multiple applications in the near infrared range. Here we present the experimental study of the emission of a passive mode-locked erbium-doped fibre laser with an amplification stage outside the cavity by means of Frequency Resolved Optical Gating (FROG) and spectral interferometry. Due to shot-to-shot instabilities, the FROG traces can be understood as the combination of two different traces, corresponding to the coherent artifact and the average pulse characteristics. We have modified a Principal Components Generalized Projections Algorithm, in order to make it able to retrieve efficiently both the coherent artifact and the average pulse. In addition, we study the temporal dependence of the polarization, showing that the pulses present time-dependent polarization with a stable spectral relative phase between the horizontal and vertical projections. Up to our knowledge, this is the first experimental study that shows the FROG measurements of unstable pulse trains associated with the coherent artifact and analyses the time-dependent polarization in ultrafast fibre lasers.

Keywords: coherent artifact; time-dependent polarization; ultrashort pulse measurement; erbium-doped fibre laser; ultrafast fibre lasers

1. Introduction

Erbium-doped fibre lasers (EDFLs) have been studied for many decades due to their great versatility and multiple applications in the near-infrared range such as telecommunication, optical sensing or microprocessing [1,2]. These lasers can operate in continuous emission or pulsed emission with interesting characteristics. In particular, passive mode-locked EDFLs are highly demanded as simple, compact and low-cost sources of ultrashort pulses in many applications such as optical coherence tomography [3], micro-welding [4] and supercontinuum generation [5].

In order to optimize the performance of a laser in a specific application, it is needed an appropriate characterization of its emission. The best scenario would be to study the individual pulses of the pulse train by using a single-shot characterization technique such as single-shot autocorrelation [6], GRENOUILLE (GRating-Eliminated No-nonsense Observation of Ultrafast Incident Laser Light E-fields) [7], SPIDER (Spectral Phase Interferometry for Direct Electric-field Reconstruction) [8] or TSHG D-scan (Transverse Second Harmonic Generation Dispersion Scan) [9]. However, due to the high repetition rate of these lasers (usually around the MHz range) and the low energy of the pulses, usually it is necessary to average the detected signal over multiple pulses even in the case of single-shot techniques. Thus, these lasers are usually characterized by multi-shot techniques such as autocorrelation, FROG (Frequency Resolved Optical Gating) or D-scan (Dispersion Scan) [10,11].

One important feature in mode-locked EDFLs is the stability. This type of lasers is usually characterized by high stability but sometimes they can operate in unstable regimes. One example of these unstable regimes is the noise-like pulses (NLP) regime, firstly reported in

EDFLs by Horowitz et al. [12]. The NLP regime consists on wave packets composed of a picosecond (ps) scale envelope comprising femtosecond (fs) scale oscillations. This regime is usually characterized by a smooth spectrum and presents a temporal autocorrelation with a narrow spike in the fs scale over a slowly varying ps structure [13–15].

Definitely, it is crucial for different applications to know if the laser design is stable or, contrarily, it presents any kind of instability. Considering that multi-shot measurements are based on the average of multiple signals from different unstable pulses, the conventional reconstruction algorithms fail to provide a truthful reconstruction when assuming a stable emission [16].

Since the last decade, it has been studied the effect of different types of instabilities using conventional characterization techniques [16–23]. In particular, recently it has been published an experimental study of instabilities in photonic-crystal fibre of a fibre laser using D-scan [19]. Regarding the FROG technique, previous works [16–18] focused on the study of FROG traces resulting from an unstable train of pulses (hereafter called CA FROG traces), so that the resulting trace can be modelled as the contribution of two auxiliary components. On one hand we have the coherent artifact (CA), and on the other hand we have the average pulse. In those papers the CA is associated to the shortest repeating substructure of the pulse train and the average pulse is referred to the temporal envelope of the average bunch of pulses. This can be understood as a way to model the unstable pulse train and a chance to extract additional information from the FROG traces. Recently, Escoto et al. [17] have proposed a modified Generalized Projections Algorithm in order to model this kind of FROG traces, from a numerical approach. Following this idea, we have developed a modified Principal Components Generalized Projections Algorithm (PCGPA) to study CA FROG traces and we have applied it to experimentally study an unstable passive mode-locked EDFL with an amplification stage outside the cavity. Moreover, in the present work we connect the experimental results from this general model with the one proposed to describe the NLP [12–15], where the average of the randomly varying fs structures can be interpreted as the coherent artifact, and the ps temporal structure can be described as the average pulse.
Besides the characterization of the system stability, it is also very important to know the polarization state of the pulses. Many characterization techniques are designed for scalar pulses, so they assume that the polarization is linear and constant in time [10]. However, the inaccurate knowledge of the time dependence of the pulse polarization could yield in drastic consequences for those applications dependent on the pulse polarization. In order to tackle this problem, for many years there have been proposed some characterization techniques able to study the polarization state of ultrafast lasers such as POLLIWOG (POLarized Light Interference versus Wavelength of Only a Glint) [24], TURTLE (Tomographic Ultrafast Retrieval of Transverse Light E-fields) [25] or time-resolved ellipsometry [26]. Moreover, it is well known that in optical fibres without maintained polarization, the state of the polarization is very sensitive to any changes in the fibre and there could be cases where the pulses present complex arbitrary polarization states. Taking this into mind, we have also applied a polarization characterization technique based on in-line interferometry [27] in order to measure the time-dependent polarization state of the passive mode-locked EDFL with an amplification stage under study.

In this paper, we present a study of the pulses of a passive mode-locked EDFL with an amplification stage outside the cavity, analysing its emission in the time domain and its stability. First, in section 2, the experimental set-up and techniques are presented (subsection 2.1), as well as the methods for the analysis of the FROG traces of unstable pulse trains with a modified PCGPA (subsection 2.2). Section 3 presents the experimental results obtained from the FROG measurements of the unstable pulse trains as a function of the amplification (subsection 3.1) and the time resolved polarization analysis of the pulsed emission (subsection 3.2). The conclusions are presented in section 4. Up to our knowledge, this is the first

experimental study that models the unstable FROG measurements and analyses the time-dependent polarization in ultrafast fibre lasers.

2. Material and Methods

2.1 Experimental set-up

The experimental set-up, as it is shown in Fig. 1, can be divided in two different parts: the laser system (blue background) and the characterization systems (orange background).

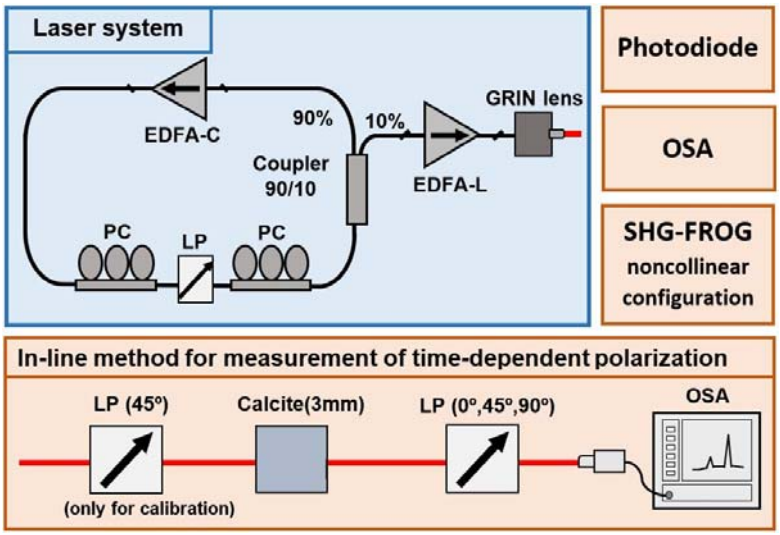

Fig. 1 Scheme of the experimental set-up: laser source (blue background) and characterization systems (orange background). The characterization systems are: photodiode for the direct observation of the pulse train, Optical Spectrum Analyser (OSA) for the spectra measurement, noncollinear SHG-FROG for temporal characterization and the in-line method for measurement of time-dependent polarization of ultrashort pulses.

The laser system was composed by an oscillator based on Er3+ doped optical fibre amplifier followed by an amplification stage outside the cavity. The oscillator was an erbium doped fibre mode-locked laser in a ring configuration with an Erbium Doped Fibre Amplifier or EDFA (EDFA-C, JDSU, model JDSU00919629) operating in the C-band (from 1530 nm to 1565 nm) with +14 dBm saturation output power as active medium. The cavity was made of standard single-mode optical fibre (Corning, model SMF-28) and the output coupler extracts a 10% of the energy (10/90 coupler). The passive mode-locking was achieved by means of the Non-linear Polarization Rotation (NPR) effect [28,29]. This effect is commonly used as a passive technique to achieve the mode-locking in fibre lasers because its effectiveness increases with the optical intensity and with the length of the fibre. In the proposed system, the optical modulator is formed by a linear polarizer (LP, Thorlabs, model ILP1550SMFC) placed between two polarization controllers (PC, Thorlabs, model FPC560). The repetition rate of the oscillator in pulsed operation was 4.37 MHz, exhibiting a spectrum centred at 1566 nm with 15.4 nm full width at half maximum (FWHM), as it is shown in Fig. 2.

Then, the pulse train coming from the oscillator is amplified by means of an EDFA operating in L-band (from 1565 nm to 1625 nm) with +20 dBm saturation output power (EDFA-L, Keopsys, model KPS-BT2-L-20-PB-FA). Moreover, its pump power can be modified allowing us to study the influence of the gain on the laser emission.

The amplified pulses were collimated into the air by means of a GRIN lens (CONCENT, model KPMC-A-250-1550-Y-20-C-FC/APC) and they were characterized by using four different systems. First, the fundamental spectra were measured with an Optical Spectral Analyzer (OSA, Agilent, model 86145B) using a spectral resolution of 0.5 nm. Second, the temporal characterization of the horizontal polarization projection (x-axis) of the generated pulses were done with a home-built SHG-FROG in noncollinear configuration (see details of this technique in subsection 2.2). The nonlinear medium used in the SHG-FROG was a 500 μm width type I BBO that ensures the phase-matching for all the spectrum generated. Third, the measurement of the time-dependent polarization of the full vector pulse was done with in-line spectral interferometry [27], allowing us to measure the difference of phase of the vector pulse between two orthogonal projections. This in-line technique consists on a bulk interferometer made of a 3 mm width calcite with the fast axis along the horizontal direction, which introduces a 1.8 ps delay in the spectral range of our laser between the horizontal (x-axis) and vertical (y-axis) polarization projections. After the interferometer, a linear polarizer is placed (LP, Newport, 10GL08) in order to select the desired projection to be measured with the OSA. Moreover, during the calibration of the technique, it is needed to place another linear polarizer at the entrance of the system with its axis at 45º, in order to study the difference of phase between both projections introduced by the characterization system.

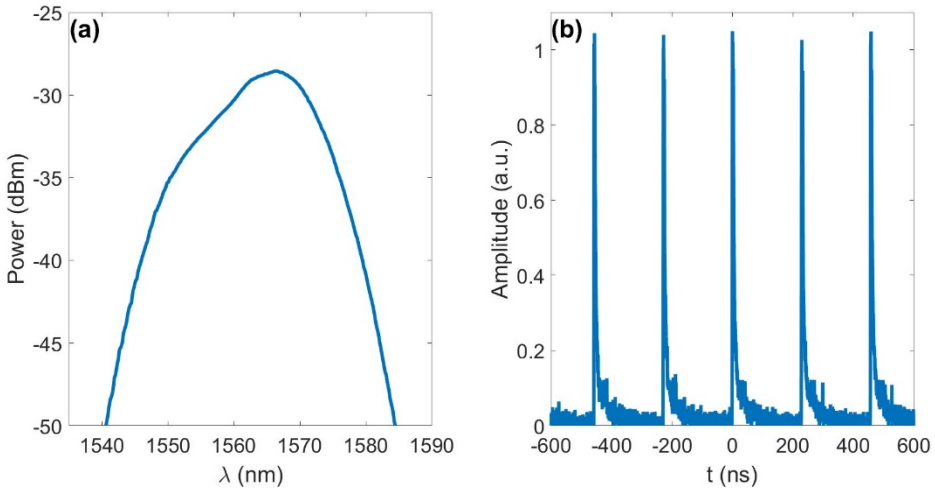

Fig. 2 Characterization of the oscillator in pulsed operation. (a) Fundamental spectrum measured with the OSA. (b) Pulse train measured with the photodiode. More details can be found in the text.

Finally, the repetition rate of the system (4.37 MHz) was measured with a photodiode (ALPHALAS, model UPD-15-IR2-FC) operating in a spectral range from 800 nm to 1700 nm with a rise time of 15 ps. It is important to point out that with the temporal resolution of this photodiode, the pulse trains seemed to be stable, as it is shown in Fig. 2b. However, as we show in this paper, using a SHG-FROG (which has better temporal resolution) it is observed that the pulse trains are unstable. This remarks the importance of an appropriate characterization of the pulses in order to avoid misunderstandings due to lack of temporal resolution.

2.2 Modified FROG reconstruction algorithm

FROG is an amplitude and phase characterization technique commonly used for ultrashort pulse temporal measurements [30]. In this paper we used one of the most common configurations, SHG-FROG in non-collinear scheme. In this set-up two non-collinear replicas of the input pulse overlap onto a nonlinear crystal for different relative delays, while the spectra of their SHG are recorded in a 2D trace called FROG trace. Provided that the pulse train is stable, it can be

reconstructed from the FROG trace using specific algorithms such as Generalized Projections [31], Principal Components Generalized Projections [32] or ptychographic algorithm [33], among others. However, there are some cases in which the conventional FROG algorithms do not converge due to instabilities in the pulse train [16]. In the last decade it has been proposed an approach to a type of unstable FROG traces, called CA FROG traces, that presents double temporal structure, based on the division of the original pulse train in two auxiliary pulses called coherent artifact and average [16–18].

Following the idea presented by Escoto et al. [17] and based on the PCGPA (Principal Components Generalized Projections Algorithm) of [34], we have developed a modified PCGPA that models the CA FROG traces produced by an unstable pulse train as the combination of two different traces, the coherent artifact (CA) trace and the average pulse trace ("ave"), as given by

$$I_{FROG}(\omega,\tau) = \Gamma I_{CA}(\omega,\tau) + (1-\Gamma) I_{ave}(\omega,\tau) \quad [1]$$

where I_{FROG}, I_{CA} and I_{ave} are respectively the FROG trace of the experimental measurement, the coherent artifact and the average pulse, all of them with the maximum normalized to unity. The variables ω and τ represent the spectral and delay dependences of the traces. The term Γ (with $0 \leq \Gamma \leq 1$) stands for the relative weight of the coherent artifact trace and the average trace in the global reconstruction.

In previous works [16–18] the CA represents the shortest repeating substructure of the pulse train, so it is imposed that the CA is a Fourier Transform Limit (FTL) pulse. In this work we propose another interpretation of the CA as the average of the fs scale variations reported in the noise-like pulses regime, letting the reconstruction algorithm to retrieve the phase of the CA without imposing any constrains. We have chosen not to impose the FTL constraint because, as it will be shown in subsection 3.1, our experiments show that the CA could be different from the FTL.

The modified PCGPA proposal was designed exclusively for CA FROG traces and should be used only if the conventional PCGPA or analogous algorithms do not converge or present high G errors (defined as the root-mean-square or rms difference between the retrieved and original FROG traces), which may be a manifestation of having unstable pulse trains [21]. Our method presents the same constrains as the usually found in a SHG FROG system (e.g. enough energy to generate the second harmonic signal, phase-matching over all the spectrum or good signal to noise ratio), but it also requires a temporal width of the average much wider than the CA temporal width in order to be able to efficiently separate the CA trace from the average pulse trace. The algorithm presents a structure divided in the different steps shown in Fig. 3.

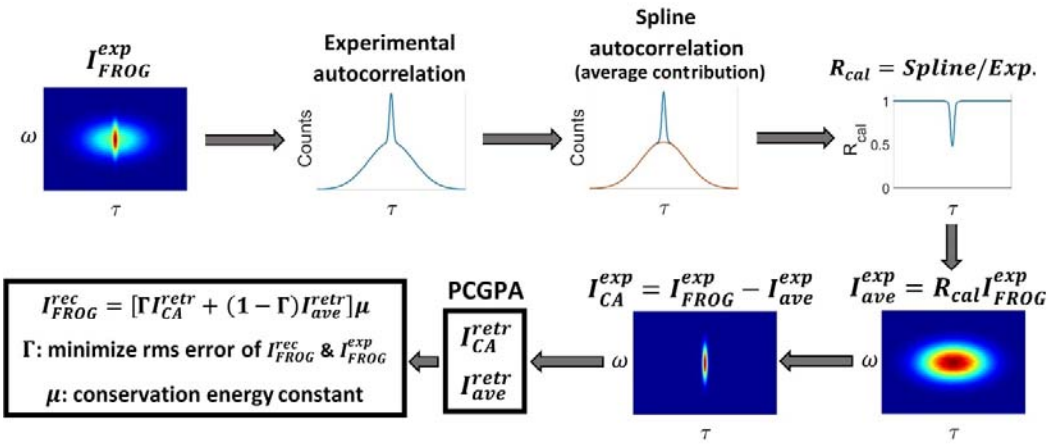

Fig. 3 Diagram of the modified PCGPA algorithm for the reconstruction of double structured FROG traces.

The algorithm uses all the FROG traces with the maximum normalized to unity. First, for a given experimental FROG trace $\left(I_{FROG}^{exp}\right)$ the algorithm calculates the intensity autocorrelation (corresponding to the delay marginal of the trace, which is integrated in the spectral axis), which for unstable pulse trains is expected to show a narrow central spike over a broader temporal basis. From this signal, the autocorrelation that the ps-scale pulse structure would generate (corresponding to the average pulse) is calculated. To do this, the central part of the experimental autocorrelation curve of the average component is estimated by spline interpolation from the basis, so the central spike can be removed. After that, it is defined a calibration function (R_{cal}) in the temporal domain, as the quotient between the spline autocorrelation (associated to the average pulse) and the experimental autocorrelation (associated to the full pulse). Next, this calibration function is applied for every frequency of the trace I_{FROG}^{exp} obtaining the contribution of the average pulse to the experimental FROG trace $\left(I_{ave}^{exp}\right)$. The contribution of the CA to the experimental FROG trace $\left(I_{CA}^{exp}\right)$ is defined as the difference between I_{FROG}^{exp} and I_{ave}^{exp}. Then, the conventional PCGPA is applied both for the I_{ave}^{exp} and I_{CA}^{exp} traces, retrieving the electric field for each case and their corresponding FROG traces, which are called I_{ave}^{retr} and I_{CA}^{retr}, respectively. Thereafter, the reconstructed FROG trace (I_{FROG}^{rec}) is defined following the equation [1] multiplied by a normalization constant (μ). This constant is defined as the quotient between the integral of the experimental and reconstructed FROG traces, and it ensures that the energies of I_{FROG}^{rec} and I_{FROG}^{exp} are the same. Finally, it is found the value of Γ that minimizes the rms error between I_{FROG}^{rec} and I_{FROG}^{exp}.

The modified PCGPA proposed was tested numerically using different FROG traces generated by unstable pulse trains composed by 5000 pulses. Those pulses were generated from a stable seed corresponding to a FTL gaussian pulse with $10\delta t$ (FWHM) temporal duration, to which it has been added a random spectral phase. Moreover, in the temporal domain each pulse is multiplied by a wide gaussian envelope in order to avoid the spreading of the signal. This numerical test is similar to the one done by Escoto et al. [17] that sets the basis for the modified method proposed in this paper. We also replicate the way of simulating unstable pulse trains from a stable oscillator, becoming unstable after adding a random spectral phase that could be introduced, for example, in a post-amplification stage.

The proposed algorithm was tested using different values ($50\delta t$, $100\delta t$, $150\delta t$) of the FWHM temporal width of the wide gaussian envelope. In Fig. 4 are compared the original (first row) and reconstructed (second row) FROG traces for each case. All the reconstructions show a good agreement with G errors lower than 0.2%, pointing out that the proposed algorithm works correctly.

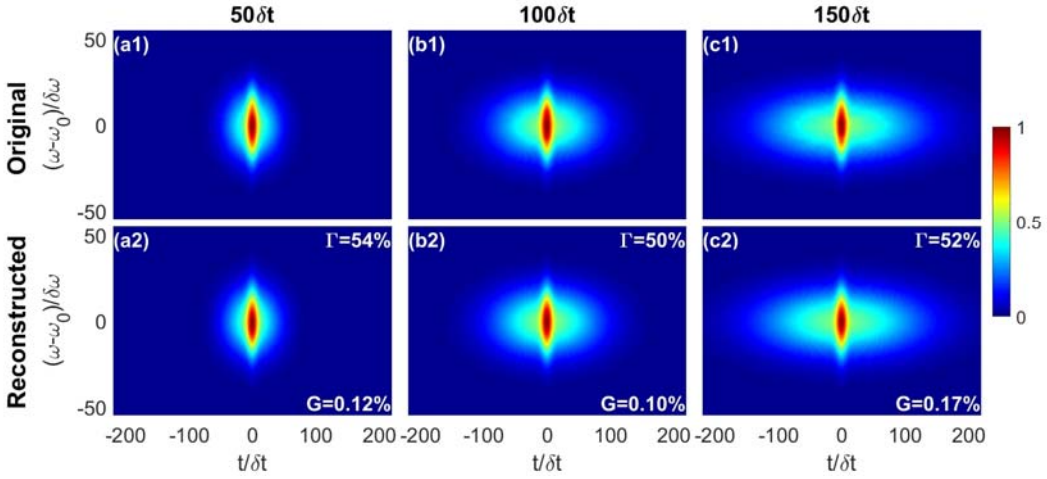

Fig. 4 Numerical test of the modified PCGPA algorithm for a seed of $10\delta t$ (FWHM) with different values of the FWHM temporal width of the temporal gaussian envelope: (a) $50\delta t$; (b) $100\delta t$;(c) $150\delta t$. First row represents the original FROG trace calculated from the unstable train. Second row shows the reconstructed FROG traces using the modified PCGPA for each case.

The good agreement between the original and reconstructed FROG traces shown in Fig. 4 is also reflected in the comparison shown in Fig. 5. On the one hand, Fig. 5a compare the reconstruction of the average pulse with the wide gaussian envelope for each case, showing a good fit between the theory and the reconstruction for the average. On the other hand, Fig. 5b compare the CA with the seed used to generate the pulse trains and it also presents a great agreement with small differences at the tails of the pulse.

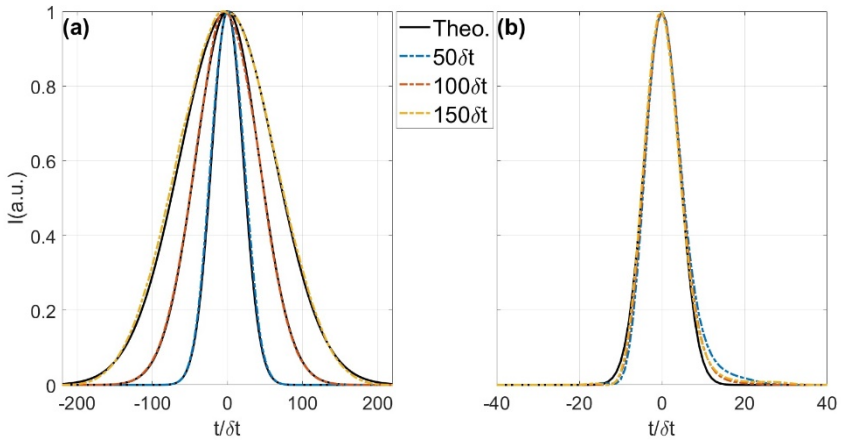

Fig. 5 Numerical comparison of the temporal evolution. (a) Average reconstruction compared with the wide gaussian envelope (Theo.) for each case. (b) CA reconstruction compared with the seed (Theo.) used to create the unstable pulse train.

The interpretation that we have proposed to the CA and the average pulses associated with the NLP regime is observed in Fig. 5. Firstly, the CA, corresponding in our definition to the average of the fs pulse structure that is randomly varying, in this case corresponds to the gaussian seed to which we are adding noise. Secondly, the average corresponding in our definition to the ps structure that involves the dynamics, corresponds in this case with the gaussian envelope that comprises the random dynamics.

Notice that in the numerical test shown in Fig. 4 and Fig. 5, the CA and the average pulses are approximately gaussian curves because we have used gaussian pulses for the simulation of the unstable pulse train (as we have previously mentioned). The modified PCGPA proposed in this paper works perfectly with other arbitrary pulse shapes too, since the CA and average retrievals are performed using a conventional PCGPA, which obtains the electric field that minimizes the rms error between the contributions to the original trace defined with our algorithm (I_{ave}^{exp} and I_{CA}^{exp}) and the individual retrievals (I_{ave}^{retr} and I_{CA}^{retr}). In fact, we have tested this analysis with sech2 pulses obtaining similar results.

3. Results and Discussion

3.1 Influence of the amplification to the unstable emission

First, we wanted to study the effect of the amplification stage to the FROG traces and the pulse train stability. Thus, for the maximum pump power of the EDFA-C and an arbitrary fixed configuration of the polarization controllers that allows the mode-locking condition, we studied the influence of the pump intensity of the EDFA-L (I_P) on the FROG traces.

Under this configuration, the measured FROG traces presented a temporal double structure as it is shown in the three examples of Fig. 6 (column a). Each row of Fig. 6 corresponds to a different value of I_P, from top to bottom 250 mA, 550 mA and 750 mA. It was impossible to achieved reasonably reconstructions with a conventional PCGPA, which was associated to retrievals presenting high FROG G errors. Therefore, we applied the modified PCGPA explained in Section 2.2 solving the problem of convergence and obtaining better reconstructions as it is shown in the column b of Fig. 6. Columns c and d of Fig. 6 show respectively the retrieved average and CA pulses pointing the weight of each trace.

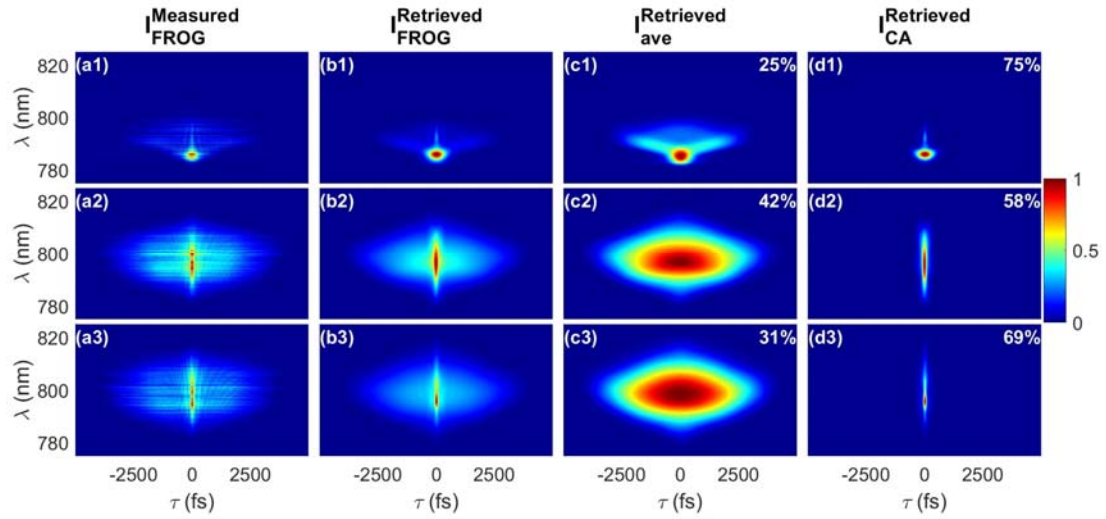

Fig. 6 FROG reconstruction measured in the same configuration but with different I_P from top to bottom: 250 mA, 500 mA and 750 mA. Experimental (column a), reconstructed (column b), average pulse (column c), and CA (column d) FROG traces for each pumping intensity. Note that all traces are individually normalized to maximum unity.

As we can see in Fig. 6 the spectral structure of the FROG traces changes as the intensity grows. Moreover, the weight of the CA trace, Γ as defined in the equation [1], also depends on the pumping intensity. The evolution of Γ with I_P is shown in Fig. 7a, where the shadowed area represents the confidence zone of the adjustment of Γ in which the deviation from the minimum value of the rms error between the experimental and reconstructed traces is lower than 5%. We

used this criterion to quantify the error of Γ, finding an acceptable experimental uncertainty except for the lowest I_P values. The dependence of the laser emission with the pumping intensity is also observed in Fig. 7b that shows the temporal width (FWHM) of the average, CA and the Fourier Transform Limit (FTL) of the experimental spectrum as a function of I_P. The elimination of the flat phase constraint in the reconstruction of the CA, used in previous works [16–18], that we have done is justified with the difference between the CA and the FTL of the experimental spectrum shown in Fig. 7b.

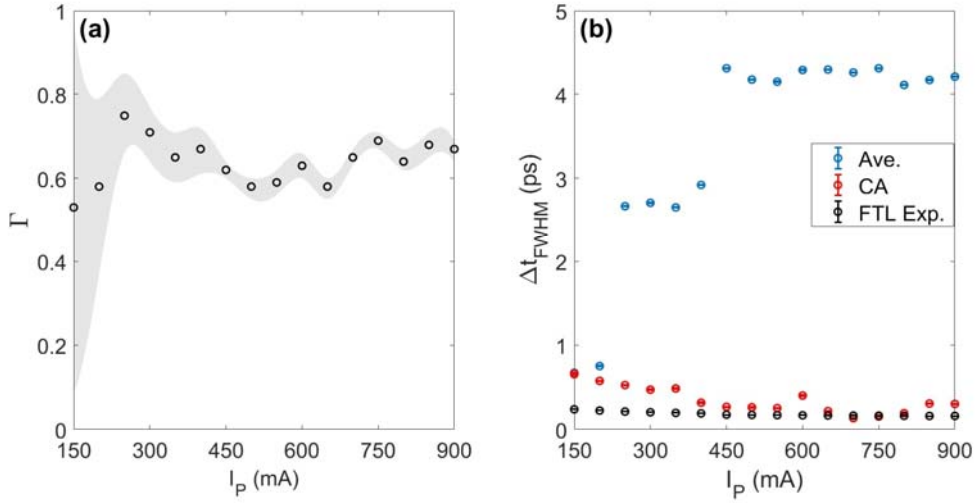

Fig. 7 Evolution of parameters as a function of the pumping intensity of the amplification stage, I_P. (a) Weight of the CA on the reconstructed traces, Γ. (b) Temporal width (FWHM) of the average (blue), CA (red) and Fourier Transform Limit of the experimental spectrum (black).

Observing Fig. 6 and Fig. 7, the emission of the laser as a function of the pumping intensity could be divided into three different regimes. Firstly, for I_P lower than 250 mA, the error in the determination of Γ is high and the temporal widths of the average and CA are close. This regime could be associated to low instability and probably the division proposed for the original pulse in CA and average is not possible. Secondly, for I_P from 250 mA up to 400 mA, the instability rises implying a reduction in the error of Γ. Moreover, in this regime the CA is closer to the FTL of the experimental spectrum and the average is much wider than the CA. Lastly, for I_P higher than 400 mA, the temporal width of the average seems to saturate, the spectrum presents the generation of new red frequencies and the error of Γ becomes very small. This regime is characterized by the predominance of the nonlinear effects, implying the creation of new frequencies and the presence of high instability. Therefore, our experimental set-up reaches a highly unstable regime for I_P above 400 mA, implying that the minimum energy per pulse required to reach this unstable regime in our experimental system is 3.8 nJ.

3.2 Vector pulse experimental study

Finally, we want to study deeper the pulsed emission of the laser paying special attention to the spectrum and the polarization status for different configurations of the polarization controllers. In Fig. 8 and Fig. 9 we present the characterization obtained for an arbitrary fixed configuration of the polarization controllers, different from the one presented in the previous subsection, that corresponds to an I_P of 550 mA.

In Fig. 8a it is represented the experimental FROG trace of the pulse train. The similarity between this experimental trace and the CA FROG traces structure, as well as the lack of

convergence of conventional PCGPA, indicate that the experimental trace could be generated due to an unstable pulse train. So we can apply the modified PCGPA previously explained, obtaining the reconstructed FROG trace shown in Fig. 8b.

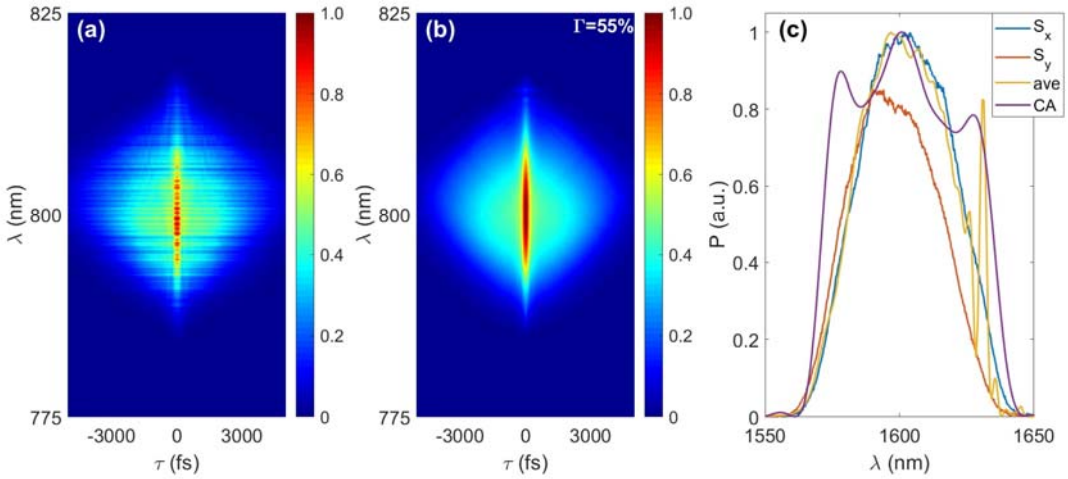

Fig. 8 Complete measurement of I_P= 550 mA. (a) Experimental FROG trace. (b) Reconstructed FROG trace with Γ =55%. (c) Spectral comparison of the horizontal (S_x) and vertical (S_y) projections of the vector pulse measured with the OSA and the spectra retrieved for the average (ave) and coherent artifact pulses (CA).

Notice that the bigger G error obtained (around 1.6%), compared with the numerical test of the PCGPA obtained in subsection 2.2 (lower than 0.2%), could be due to the noisy spectral structure of the original trace that is not presented in the reconstruction and it also does not appear in the numerical simulations. Despite this higher G error, the agreement between the traces is very good. The parameter Γ in this case is 55%, implying that the pulse train is highly unstable because the contribution of the CA is not negligible. This corroborates that the laser is an unstable system where the pulse to pulse emission changes and the average and coherent artifact are a way of modelling or extracting some information about the laser emission. This is also revealed in Fig. 8c because none of the spectra, neither the CA nor the average, fits exactly with the experimental spectrum of the x-polarization projection (S_x) that was characterized with the FROG. In spite of the differences, in this particular case the average spectrum is similar to the experimental one, but this is not a general behaviour as corroborated by other measurements.

In addition to the FROG analysis, it was also studied the polarization of the pulse train with the method reported in [27]. Fig. 9a and Fig. 9b show the reconstructed temporal evolution of the electric field, associated to the average pulse and the CA respectively, as a function of the ellipticity defined as the minor to major axes ratio. Additionally, Fig. 9c and Fig. 9d show, for the average and CA respectively, the temporal evolution of: the total intensity (I_T), the orientation of the polarization ellipse to the x-axis (azimuthal angle χ) and the redefined ellipticity ($\epsilon_r = \text{sign}(\delta) \cdot \epsilon$) defined as the ellipticity multiplied by the sign of the phase difference between the x and y components (δ). The sign of the redefined ellipticity indicates the helicity, so if $\epsilon_r > 0$ it is right-handed or if $\epsilon_r < 0$ it is left-handed.

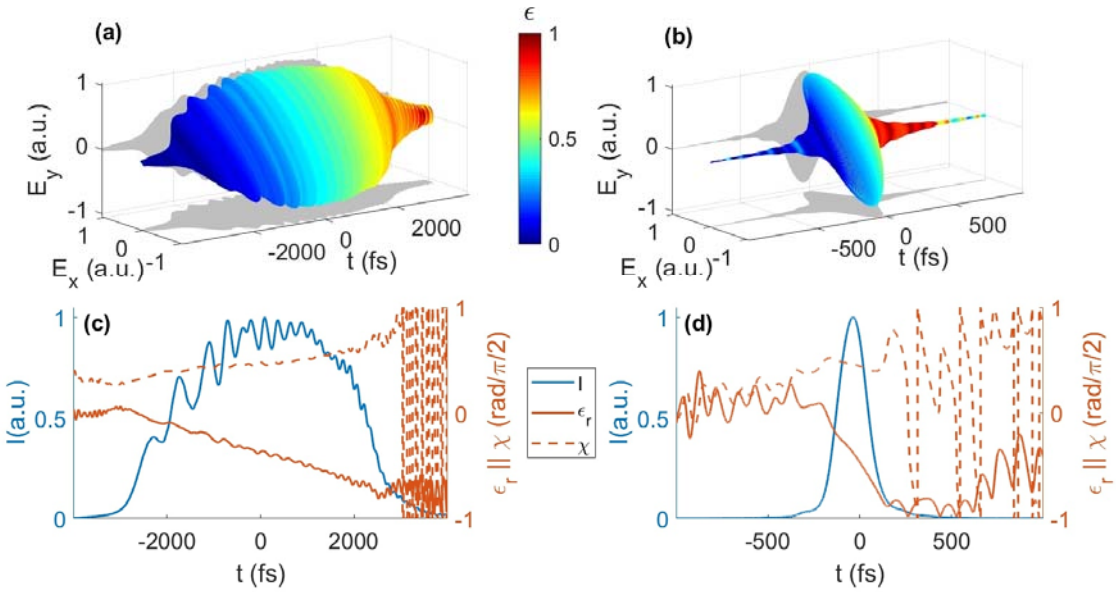

Fig. 9 Polarization results for the average (left column) and CA (right column). Upper row shows the time dependent evolution of the electric field as a function of the ellipticity (ϵ). Lower row shows the time dependency of the total intensity (I), redefined ellipticity (ϵ) and azimuth (χ).

In order to evaluate the contrast of the interferences, we have calculated the pure interference term (without the contribution of each projection spectra) obtaining that the weight is 88%. Notice that, in spite of the shot-to-shot fluctuation, there is good contrast of the interferential fringes. It could be only explained by the conservation or presence of small changes in the relative phase between the orthogonal projections of the vector pulse generated by the laser. Moreover, the polarization state is changing along the pulse as it is shown in Fig. 9. This implies that the pulses generated by the fibre system have time-dependent polarization. This idea was tested with many other configurations of the polarization controllers and intensities of the EDFA-L20 and it was found that all of them showed different time dependent polarization.

As we have discussed along the paper, the division of the FROG measurement in CA and average pulses is just a way of modelling the unstable train, in order to extract some information. Taking this into mind we have associated the characterization to both pulses showing the vector nature of the pulses generated with the fibre laser. The main differences between both reconstructions in the case represented in Fig. 9 are the temporal width and the small undulation of the average pulse. The origin of the undulation is the small modulation presented in the measured spectral amplitude (Fig. 8c). This modulation becomes evident in the temporal domain due to the pulse stretching caused by a strongly chirped pulse, and this is the reason why it is only seen in the average pulse. Despite these differences, it is clear that the pulses generated by the fibre laser present a vector behaviour. This could be originated due to the anisotropy of the fibre and, if it is the case, it would likely appear even in stable cases. Therefore, it is necessary a vector study in order to completely characterize the emission of pulsed fibre lasers.

4. Conclusion

In this work we have studied a passive mode-locked erbium doped fibre laser with an amplification stage exhibiting an unstable emission in the time domain. In order to study the SHG FROG traces of the unstable laser, we have implemented a Principal Components

Generalized Projections FROG reconstruction algorithm, which is able to model experimental FROG traces as the sum of two different traces, namely the coherent artifact (CA) and the average pulse contributions. We have observed that the different behaviour of the laser emission can be due to different regimes of instability, reaching a highly unstable regime in which the method proposed presents a better performance, for pulse energies over 3.8 nJ. Up to our knowledge, this is the first experimental study of double structured FROG traces related to an unstable optical fibre laser emission in the near-infrared region.

Furthermore, the pulsed emission of our laser system has been also characterized in terms of the polarization stability of the pulse train, finding that the polarization state changes along the pulse maintaining a stable spectral relative phase between the horizontal and vertical projections.

Finally, we want to point up the importance of a complete characterization of the fibre lasers used in many different applications, and to show that the usually stable fibre lasers could present a complex emission with shot-to-shot fluctuations and also time dependent polarization.

Funding: This work was supported by the Ministerio de Economía y Competitividad (EQC2018-004117-P, FIS2017-87970-R); the Consejería de Educación, Junta de Castilla y León (SA287P18, SA136P20); the Consejería de Educación de la Junta de Castilla y León (VA085G19); and the INTERREG V-A España-Portugal (POCTEP) program (0677_ DISRUPTIVE _ 2_ E)

References

[1] Milione G, Nguyen TA, Leach J, Nolan DA, Alfano RR. Using the nonseparability of vector beams to encode information for optical communication. Optics Letters 2015;40:4887–90. https://doi.org/10.1364/ol.40.004887.

[2] Shi W, Fang Q, Zhu X, Norwood RA, Peyghambarian N. Fiber lasers and their applications [Invited]. Applied Optics 2014;53:6554–68. https://doi.org/10.1364/ao.53.006554.

[3] Nishizawa N, Chen Y, Hsiung P, Ippen EP, Fujimoto JG. Real-time, ultrahigh-resolution, optical coherence tomography with an all-fiber, femtosecond fiber laser continuum at 15 μm. Optics Letters 2004;29:2846–8. https://doi.org/10.1364/ol.29.002846.

[4] Tamaki T, Watanabe W, Itoh K. Laser micro-welding of transparent materials by a localized heat accumulation effect using a femtosecond fiber laser at 1558 nm. Optics Express 2006;14:10460–8. https://doi.org/10.1364/oe.14.010460.

[5] López-Ripa M, Jarabo S, Salgado-Remacha FJ. Near-infrared supercontinuum source by intracavity silica-based highly-nonlinear fiber. Optics Letters 2019;44:2016–9. https://doi.org/10.1364/OL.44.002016.

[6] Salin F, Georges P, Roger G, Brun A. Single-shot measurement of a 52-fs pulse. Applied Optics 1987;26:4528–31. https://doi.org/10.1364/ao.26.004528.

[7] O'Shea P, Kimmel M, Gu X, Trebino R. Highly simplified device for ultrashort-pulse measurement. Optics Letters 2001;26:932–4. https://doi.org/10.1364/ol.26.000932.

[8] Iaconis C, Walmsley IA. Spectral phase interferometry for direct electric-field reconstruction of ultrashort optical pulses. Optics Letters 1998;23:792–4. https://doi.org/10.1364/OL.23.000792.

[9] Salgado-Remacha FJ, Alonso B, Crespo H, Cojocaru C, Trull J, Romero R, et al. Single-shot d-scan technique for ultrashort laser pulse characterization using transverse second-harmonic generation in random nonlinear crystals. Optics Letters 2020;45:3925–8. https://doi.org/10.1364/ol.397033.

[10] Walmsley IA, Dorrer C. Characterization of ultrashort electromagnetic pulses. Advances in Optics and Photonics 2009;1:308–437. https://doi.org/10.1364/aop.1.000308.

[11] Miranda M, Arnold CL, Fordell T, Silva F, Alonso B, Weigand R, et al. Characterization of broadband few-cycle laser pulses with the d-scan technique. Optics Express 2012;20:18732–43. https://doi.org/10.1364/oe.20.018732.

[12] Horowitz M, Barad Y, Silberberg Y. Noiselike pulses with a broadband spectrum generated from an erbium-doped fiber laser. Optics Letters 1997;22:799–801. https://doi.org/10.1364/ol.22.000799.

[13] Pottiez O, Grajales-Coutiño R, Ibarra-Escamilla B, Kuzin EA, Hernández-García JC. Adjustable noiselike pulses from a figure-eight fiber laser. Applied Optics 2011;50:E24–31. https://doi.org/10.1364/AO.50.000E24.

[14] North T, Rochette M. Raman-induced noiselike pulses in a highly nonlinear and dispersive all-fiber ring laser. Optics Letters 2013;38:890–2. https://doi.org/10.1364/ol.38.000890.

[15] Runge AFJ, Aguergaray C, Broderick NGR, Erkintalo M. Coherence and shot-to-shot spectral fluctuations in noise-like ultrafast fiber lasers. Optics Letters 2013;38:4327–30. https://doi.org/10.1364/ol.38.004327.

[16] Rhodes M, Steinmeyer G, Ratner J, Trebino R. Pulse-shape instabilities and their measurement. Laser and Photonics Reviews 2013;7:557–65. https://doi.org/10.1002/lpor.201200102.

[17] Escoto E, Jafari R, Trebino R, Steinmeyer G. Retrieving the coherent artifact in frequency-resolved optical gating. Optics Letters 2019;44:3142–5. https://doi.org/10.1364/ol.44.003142.

[18] Escoto E, Jafari R, Steinmeyer G, Trebino R. Linear chirp instability analysis for ultrafast pulse metrology. Journal of the Optical Society of America B 2020;37:74–81. https://doi.org/10.1364/josab.37.000074.

[19] Alonso B, Torres-Peiró S, Romero R, Guerreiro PT, Almagro-Ruiz A, Muñoz-Marco H, et al. Detection and elimination of pulse train instabilities in broadband fibre lasers using dispersion scan. Scientific Reports 2020;10:7242. https://doi.org/10.1038/s41598-020-64109-x.

[20] Li Y, Lester LF, Chang D, Langrock C, Fejer MM, Kane DJ. Characteristics and instabilities of mode-locked quantumdot diode lasers. Optics Express, vol. 21, Optical Society of America; 2013, p. 8007–17. https://doi.org/10.1364/oe.21.008007.

[21] Rhodes M, Guang Z, Trebino R. Unstable and multiple pulsing can be invisible to ultrashort pulse measurement techniques. Applied Sciences (Switzerland) 2017;7:40. https://doi.org/10.3390/app7010040.

[22] Rasskazov G, Lozovoy V v., Dantus M. Spectral amplitude and phase noise characterization of titanium-sapphire lasers. Optics Express 2015;23:23597–602. https://doi.org/10.1364/oe.23.023597.

[23] Lozovoy V v., Rasskazov G, Pestov D, Dantus M. Quantifying noise in ultrafast laser sources and its effect on nonlinear applications. Optics Express 2015;23:12037–44. https://doi.org/10.1364/oe.23.012037.

[24] Walecki WJ, Fittinghoff DN, Smirl AL, Trebino R. Characterization of the polarization state of weak ultrashort coherent signals by dual-channel spectral interferometry. Optics Letters 1997;22:81–3. https://doi.org/10.1364/ol.22.000081.

[25] Schlup P, Masihzadeh O, Xu L, Trebino R, Bartels RA. Tomographic retrieval of the polarization state of an ultrafast laser pulse. Optics Letters 2008;33:267–9. https://doi.org/10.1364/ol.33.000267.

[26] Jellison GE, Lowndes DH. Time-resolved ellipsometry measurements of the optical properties of silicon during pulsed excimer laser irradiation. Applied Physics Letters 1985;47:718–21. https://doi.org/10.1063/1.96014.

[27] Alonso B, Sola I. Measurement of Ultrashort Vector Pulses from Polarization Gates by In-Line, Single-Channel Spectral Interferometry. IEEE Journal of Selected Topics in Quantum Electronics 2019;25:8900307. https://doi.org/10.1109/JSTQE.2019.2906266.

[28] Chang CW, Chi S. Mode-locked erbium-doped fibre ring laser using nonlinear polarization rotation. Journal of Modern Optics 1998;45:355–62. https://doi.org/10.1080/09500349808231694.

[29] Zhang ZX, Xu K, Wu J, Hong XB, Lin JT. Two different operation regimes of fiber laser based on nonlinear polarization rotation: Passive mode-locking and multiwavelength emission. IEEE Photonics Technology Letters 2008;20:979–81. https://doi.org/10.1109/LPT.2008.923549.

[30] Trebino R, Kane DJ. Using phase retrieval to measure the intensity and phase of ultrashort pulses: frequency-resolved optical gating. Journal of the Optical Society of America A 1993;10:1101–11. https://doi.org/10.1364/josaa.10.001101.

[31] DeLong KW, Kohler B, Wilson K, Fittinghoff DN, Trebino R. Pulse retrieval in frequency-resolved optical gating based on the method of generalized projections. Optics Letters 1994;19:2152–4. https://doi.org/10.1364/ol.19.002152.

[32] Kane DJ, Rodriguez G, Taylor AJ, Clement TS. Simultaneous measurement of two ultrashort laser pulses from a single spectrogram in a single shot. Journal of the Optical Society of America B 1997;14:935–43. https://doi.org/10.1364/josab.14.000935.

[33] Sidorenko P, Lahav O, Avnat Z, Cohen O. Ptychographic reconstruction algorithm for frequency-resolved optical gating: super-resolution and supreme robustness. Optica 2016;3:1320–30. https://doi.org/10.1364/optica.3.001320.

[34] Byrnes S. Frequency-resolved optical gating (FROG) (https://www.mathworks.com/matlabcentral/fileexchange/34986-frequency-resolved-optical-gating-frog), 2020.